This document was prepared in conjunction with work accomplished under Contract No. DE-AC09-96SR18500 with the U. S. Department of Energy.

DISCLAIMER

Submitted to ASME Pressure Vessels and Piping Conference, July 23-27, 2006, Vancouver, British Columbia, Canada

Paper Number: PVP2006-ICPVT11-93274

PREDICTING TRITIUM AND DECAY HELIUM EFFECTS ON BURST PROPERTIES OF PRESSURE VESSELS

P. S. Lam, M. J. Morgan, K. J. Imrich, and G. K. Chapman
Materials Science and Technology
Savannah River National Laboratory
Aiken, SC 29808

ABSTRACT

Burst testing is used to assess the performance of stainless steel pressure vessels designed to contain tritium, a radioactive isotope of hydrogen. Burst ductility of tritium-exposed vessels is reduced in time as a result of the combined embrittlement effects from tritium that has diffused into the microstructure and its radioactive decay product, helium-3. A materials system model and finite element procedure were developed to predict burst pressure and the vessel volume change (ductility) during burst testing. The model is used to predict changes in burst pressure and ductility from the tritium service history, known values of tritium diffusivity, and published data on the effects of tritium and helium on the tensile properties of stainless steel. Good agreement has been achieved with actual burst test data for unexposed vessels. It is shown that the service history could be used to derive values of tritium concentration in the metal and the depth of penetration in the vessel sidewall. These values could be used in the finite element model to predict values of burst pressure and burst ductility for tritium-exposed vessels.

INTRODUCTION

The burst test is an industry standard approach to evaluate pressure vessel/pipeline design and weld joint performance. In the case of storage vessels containing tritium (radioactive isotope of hydrogen), the burst test is an established protocol in evaluating the material performance after extended tritium service, from which tritium decays into a non-radioactive isotope of helium, helium-3.

The ductility of the tritium-aged material is significantly reduced as a result of helium-3 precipitated in the microstructure of the metal due to tritium decay, in addition to the effect of hydrogen (tritium) embrittlement. However, the burst testing for previously loaded vessels is very difficult and costly because of challenges associated with tritium off-gas and contamination control. As a result, it is desirable that an analytical/numerical technique be developed to complement, or even provide an alternative to, the burst testing. The method should be capable of predicting the burst pressure, and more

importantly, the volume ductility which is a measurement of the change in volume of the vessel at burst failure.

The first part of the paper describes the development of the model, analytic procedure, and material data for predicting vessel burst performance. The tensile specimens were harvested from unexposed vessels by using Electric Discharge Machining (EDM). Because the tensile specimens are curved, the test data must be adjusted. The procedure is described in the paper. This set of material properties was used to benchmark the burst test of an unexposed vessel. It can be shown that the finite element result is in good agreement with the burst test data when the stress-strain curve was scaled so the yield stress is 434 MPa (63 ksi), within the acceptable range of forged stainless steel (Type 316L). The actual failure location coincides with the calculated location of maximum Mises stress or maximum plastic strain. A strain-based failure criterion is proposed, that is, the volume ductility is proportional to the maximum equivalent plastic strain that occurs in the sidewall. However, a complete material database including the aged material properties are needed to validate the proposed failure criterion for a specific tritium vessel.

The second part of this paper describes the approach of evaluating tritium-aged materials to facilitate input into the model. In the absence of actual tensile properties for the exposed material, a set of simplified stress-strain relationships was obtained based on literature data in terms of the helium-3 concentration in the metal. However, to account for the formation of the mudflat cracks, which are typically found in the post-test examination on the inner fracture surface of the tritium-exposed vessels, and to postulate that these cracks may be initiated at the yield stress of the exposed material under internal pressure loading, an elastic-perfectly plastic behavior (i.e., nonhardening) is assumed. The results show that the burst pressures are similar for various exposure levels but the reduction of volume ductility has changed significantly when higher helium concentration is accumulated in the metal.

Since the tritium and helium profiles in the vessel wall are sensitive to the loading and service histories of the vessel, the burst properties (pressure and volume ductility) may be vessel dependent. Finite element analysis using vessel-specific models is proposed when the exposed tensile properties are available.

BENCH-MARKING UNEXPOSED VESSEL BURST TEST

Material Testing and Tensile Properties

The material of construction of the vessels under consideration in this paper is a forged austenitic stainless steel of type 316L, which has a yield strength in the range of 379 to 517 MPa (55 to 75 ksi, note that the yield strength of a typical annealed stainless steel is about 207 MPa or 30 ksi). The minimum ultimate tensile strength (UTS) is 586 MPa (85 ksi). Using the standard round tension test specimen as specified in American Society for Testing and Materials (ASTM) E 8 Standard Test Methods for Tension Testing of Metallic Materials (12.7 mm or 0.5 in. diameter with 50.8 mm or 2 in. gage length), the elongation and the reduction of area should meet, respectively, 35% and 40%.

Tensile specimens from a mock, non-exposed tritium vessel were harvested in the longitudinal and transverse directions with respect to the orientation of the vessel using an EDM. As seen from Figure 1, the specimens are curved with a typical thickness of 0.58 mm (0.023 in.), which was chosen to obtain averaged tensile properties of tritium and helium-bearing material. The specimen width and the reduced section length are 1.57 mm (0.062 in.) and 7.62 mm (0.3 in.), respectively. The dimensions of the specimens were chosen to minimize the curvature effects for the load frame. Both longitudinal and transverse tensile specimens were tested. A typical stress-strain curve for the longitudinal specimen (from Specimen R2SL-2 No. 33) is shown in Figure 2. The initial portion of the stress-strain data (see Fig. 2) were affected by the specimen curvature. This effect is accounted for and the actual tensile flow curve is recovered by the procedure described in the next section. The corrected engineering stress-engineering strain curve (Fig. 3) can be converted to the true measures (Fig. 4) for analyses involving large deformation such as in the event of burst test.

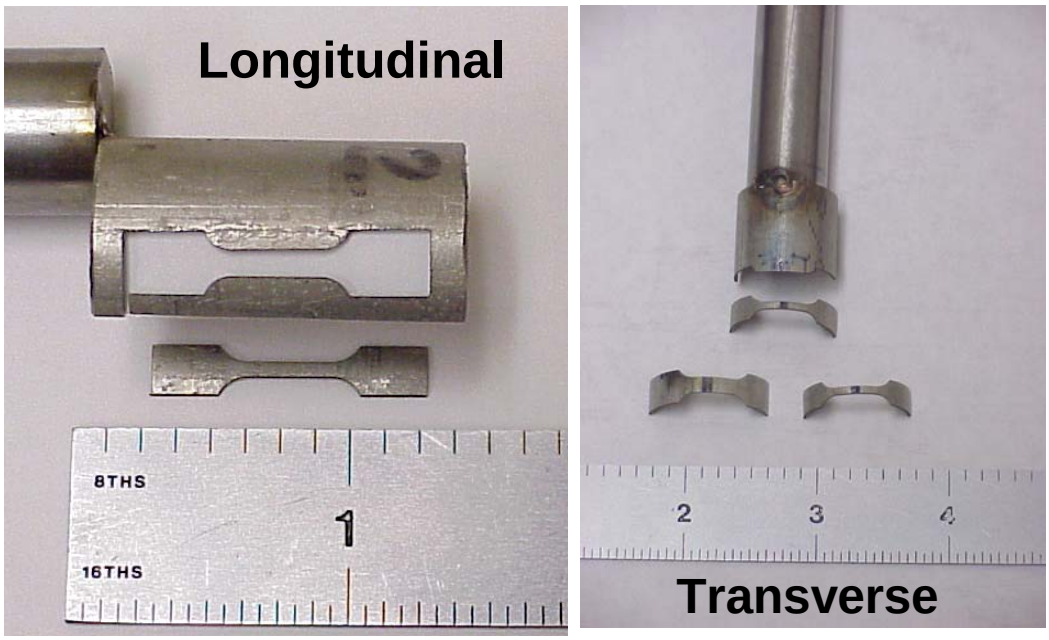

Figure 1 Typical longitudinal and transverse tensile specimens harvested from a mock, non-exposed tritium vessel using EDM

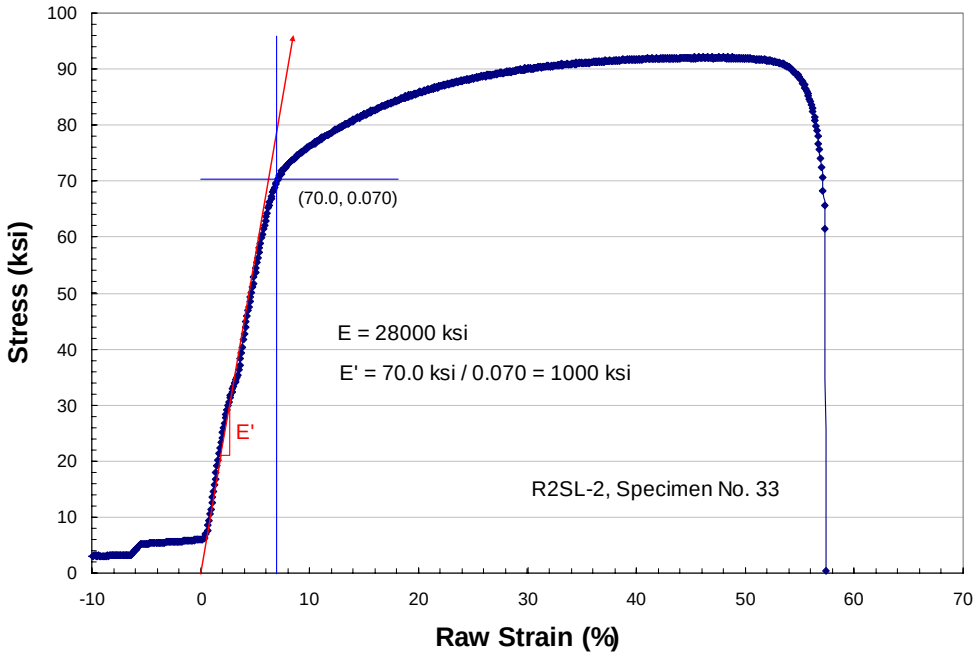

Figure 2 Engineering stress-engineering strain curve as-tested from a slightly curved tensile specimen

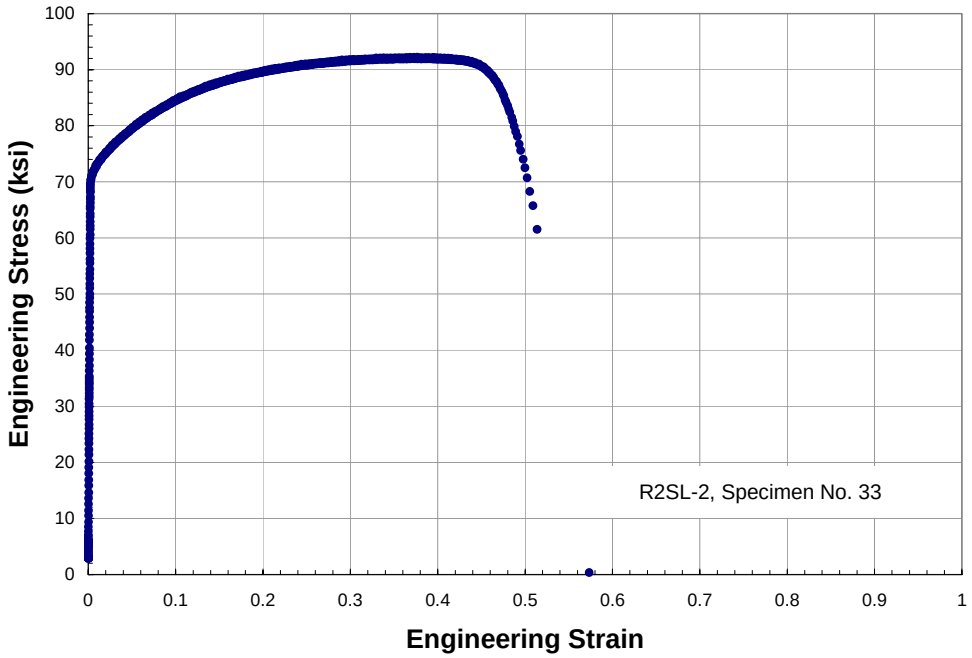

Figure 3 Corrected engineering stress-engineering strain curve

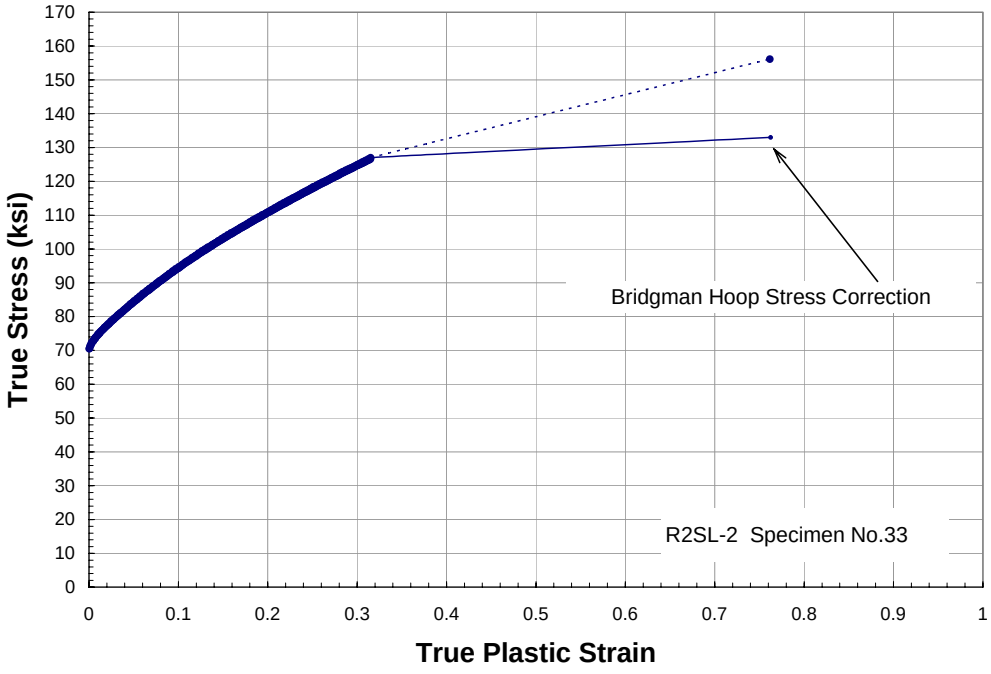

Figure 4 True stress-true strain curve and Bridgman correction for the failure point

Adjustment for Tensile Test Data

The procedure for correcting the initial portion of the stress-strain curve, and the subsequent conversion to the true stress-true strain curve with Bridgman hoop stress correction for the failure stress and strain are described in the following:

1. The standard Young's modulus (or the modulus of elasticity) for stainless steels (193 GPa or 28,000 ksi) is used for all specimens because this value is in general insensitive to this class of metallic materials at room temperature. The tensile tests performed in this study were not optimized or designed for the determination of the Young's modulus at very small strain range.
2. A straight line is identified in the initial portion of the engineering stress-engineering strain curve (see Fig. 2). Note that the slope of the line (E')is different from the Young's modulus (E), which is set to 193 GPa (28,000 ksi). The stress value at which the stress-strain curve begins to deviate from the initial straight line is considered as the yield stress of the material at zero plastic strain (the definition is different from the standard 0.2% offset yield stress).
3. The plastic deformation is defined as the total deformation minus the "as-tested" elastic deformation. In terms of engineering stress and engineering strain, it is defined as $\varepsilon_{pl}^{E} = \varepsilon_{tot}^{E} - \sigma^{E} / E'$, where ε_{pl}^{E} is the engineering plastic strain, ε_{tot}^{E} is the total engineering strain from the test data, σ^{E} is the engineering stress, and E' is measured from the slope of the initial straight line in Figure 2.
4. The actual elastic strain (ε_{el}^{E}) is defined in the traditional manner. That is $\varepsilon_{el}^{E} = \sigma^{E} / E$, where E is the standard Young's modulus of the material.
5. The corrected total engineering strain (ε_{tot}^{corr}) is therefore defined as $\varepsilon_{tot}^{corr} = \varepsilon_{el}^{E} + \varepsilon_{pl}^{E}$
6. After the strains are corrected, Figure 2 can be re-plotted as in Figure 3.
7. By standard conversion, Figure 3 is then re-plotted as the true stress (σ)-true total strain (ε_{tot}^{T}) curve. This is necessary for the large deformation finite element analysis, for example, using the ABAQUS code [1], in which the true stress-true-plastic strain curve is used (Fig. 4). The true plastic strain (ε_{pl}) is defined as $\varepsilon_{pl} = \varepsilon_{tot}^{T} - \sigma / E$
8. In Figure 4, the true stress-true plastic strain curve, any data point after necking takes place, or beyond the ultimate tensile strength (UTS) where the maximum uniform elongation occurs, should be corrected because the stress state is no longer uniaxial. For practical purpose, all the data points after UTS are discarded except the failure point, for which the final cross-sectional area of the test specimen can be measured. The original Bridgman correction [2] for the round bar tensile specimens are formulated as $\sigma_f = P_f \left(\pi R_f^2 \left(1 + 2R_N / R_f\right) \ln\left(1 + R_f / 2R\right)\right)^{-1}$ where σ_f is the (true) failure stress, P_f is the load at failure, R_f is the final measured gage section radius, and R_N is the measured radius of curvature of the

necking region. The true strain at failure based on the reduction of area is calculated by

$$\varepsilon_f^T = 2\ln(R_o / R_f)$$

where R_o is the undeformed radius of the gage section.

Instead of using the original Bridgman formulation, a simplified correction [3,4] that employed an empirical curve developed by Bridgman for steels was used:

$$\sigma_B^T = B\sigma$$

where σ_B^T is the corrected true stress, σ is the true stress calculated as the load per unit current cross-sectional area, and

$$B = 0.83 - 0.186\log\varepsilon_{tot}^T \text{ for } 0.15 \le \varepsilon_{tot}^T \le 3$$

No correction is needed for $\varepsilon_{tot}^T < 0.15$. Note that in the above expression, log is the 10-based logarithm. This simplified method is suitable for the flat specimens with rectangular cross-sections.

As an example, the failure point in the stress-strain curve is corrected as shown in Figure 4 (solid curve), which can be readily used in the large deformation finite element analysis, such as the burst test prediction in this paper. For this study, only the unexposed mechanical properties for this type of vessel steel were available. Additional testing for tritium aged specimens has recently been conducted and will be included in future analysis.

Finite Element Analysis

The burst test analysis involves both material nonlinearity (beyond linear elasticity) and deformation nonlinearity (large strains involving higher order displacement gradients) . A full stress-strain curve is generally required (Fig. 4). The Riks algorithm was developed for this type of analysis where an equilibrium solution is required for the unstable state. This algorithm is available in the ABAQUS Standard [1] for static analysis. With available laboratory-controlled burst tests for mock-up pipes and actual vessels, the finite element analysis was performed to 1) verify the deformation shape; 2) predict the failure location; 3) compare the calculated pressure-volume relationship to the measured data; and 4) develop failure criteria for predictive testing.

Finite Element Model

The configurations of the tritium vessels[1] and the mockup pipes allow an axisymmetric finite element analysis[2] to be employed. To compare with the test data, it is important to

[1] The test specimens are prototypical and are not vessels in production.

[2] For exposed tritium vessel, the post-test metallographic analysis found that mudflat cracks occurred in the inside wall of the vessel. If the cracks are considered explicitly in the finite element analysis, the axisymmetric models can not be used. In the current continuum approach, the axisymmetric analysis is appropriate.

obtain the instantaneous volume change during pressurization. This is achieved by implementing the hydrostatic fluid elements in the ABAQUS analysis [1]. Incompressible hydraulic fluid behavior is assumed. These hydrostatic fluid elements (FAX2) are attached to the standard axisymmetric elements (CAX4) of the pressure vessel (vessel) inside wall. Both the fluid pressure and the cavity volume can be monitored during the deformation.

Most of the results in this paper for a prototypic test vessel were obtained from a model with 705 elements and 719 nodes. There are 5 elements across the thickness of the vessel sidewall. A larger model consisting of 3544 elements and 3564 nodes with 20 elements across the sidewall was also used to investigate the mesh sensitivity. It was concluded that the coarser mesh provided sufficient accuracy and was appropriate in this study.

Comparison of Deformation and Prediction of Failure Location

A deformed finite element mesh at the predicted burst pressure was superimposed on the photograph of a burst mockup pipe. Figure 5 shows that the calculated shape agrees well with the post-burst specimen.

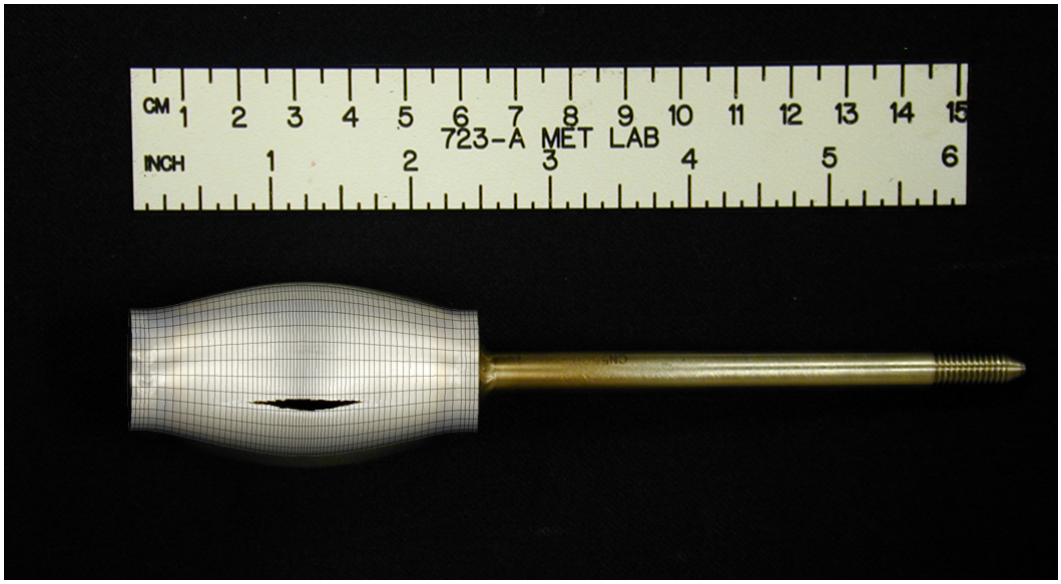

Figure 5 Post-burst configuration of a mockup pipe

The Mises stress contours are plotted over the deformed shapes of several prototypic test specimens subject to burst test in Figures 6a, b, and c. The warmer colors represent

higher stress levels and coincide with the locations of failure. In general, the failure location is in the middle of the sidewall with uniform thickness, as can be seen in the photograph in Figure 5. However, as shown in Figure 6c, when a thinner cap was fabricated for the test specimen, the failure occurs in the cap region. This has been verified experimentally.

Comparing the contour plots of the Mises stress and the corresponding equivalent plastic strain (PEEQ in ABAQUS [1]), it can be concluded that the stress or strain criterion would be equivalent in predicting failure in a burst test. However, the strain-based criterion may be favorable since the strains can be measured directly. Furthermore, stress variation is relatively insensitive near the moment of failure due to the nature of the stress-strain curve, while the strains varies significantly and can be identified easily.

The contour plots also reveal that the high stress/strain first occurs in the inside wall of the test specimen. This implies that the material fails first inside the cavity, then the failure propagates outward in a catastrophic manner. Note that the current finite element analysis is not designed for predicting post-failure configuration, including the size of rupture.

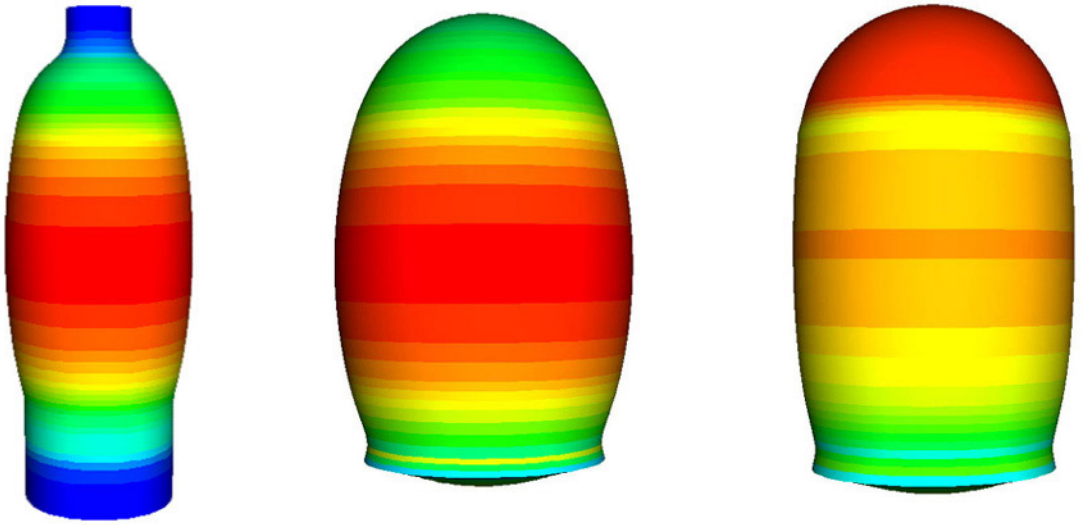

Figure 6 Mises stress contours for prototypic burst test specimens with various designs: (a) small vessel, (b) large vessel; and (c) large vessel with a thin cap

Comparison of Finite Element Prediction and Test Data

Burst test data of two prototypic vessels are plotted in Figure 7 in terms of volume ductility defined as $\Delta V/V_o$, where ΔV is the volume change and V_o is the original volume. It should be noted that there is a slight difference in defining volume: in the finite element analysis, ΔV or V_o are referred to the cavity of the vessel where the pressure is applied, while in the actual test, it is based on the entire volume of the test specimen as is measured directly by, for example, the displaced fluid in the test chamber. However, it is believed that the difference in volume change is within the inherent experimental error band because the majority of the deformation occurs in the cavity of the specimen.

When the stress-strain curve in Figure 4 (the yield stress is 483 MPa or 70 ksi) was used in performing the finite element analysis, the calculated result overestimated the experimental data. As noted earlier, the stress-strain curve was obtained from specimens harvested from prototypic tritium vessels, which were made of the same type of forged stainless steel with wide range of acceptability in fabricating the vessels, that is, the yield stress can range from 379 to 517 MPa (55 to 75 ksi). Because the tensile properties of the actual burst test specimens were not determined, the stress-strain curve in Figure 4 was scaled down to have a yield stress of 434 MPa (63 ksi), which is within the range of acceptable yield stress. Based on the adjusted stress-strain curve (see the inset of Figure 7), the finite element result agrees well with the test data as shown in Figure 7.

It should be mentioned that the peak pressure in Figure 7 before the curve bends over represents the burst pressure, and the corresponding value of $\Delta V/V_o$ is the volume ductility at failure. The volume ductility is widely used as an index for material performance in tritium-loaded and aged vessels.

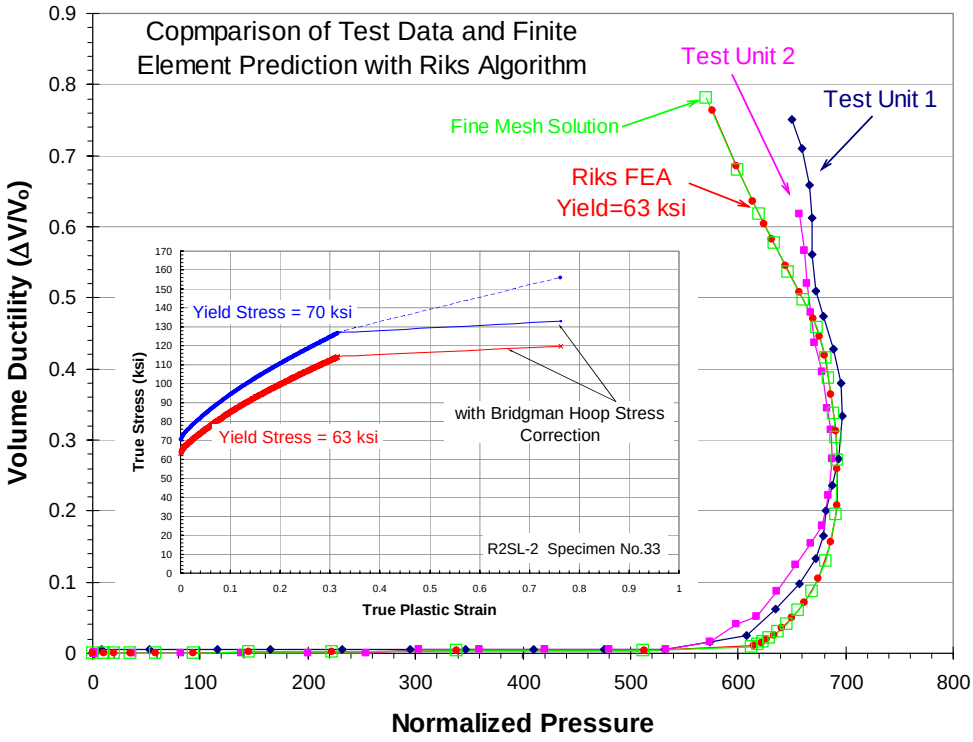

Figure 7 Comparison of the actual test data and the finite element prediction using a stress-strain curve with yield stress scaled to 434 MPa (63 ksi)

Failure Criterion for Burst Prediction

It was noted in the tests that the burst pressure is less sensitive to the material property change caused by tritium exposure and decay than the burst volume ductility. However, the volume ductility ($\Delta V/V_o$) is observed to be significantly influenced by the presence of tritium and helium. As a result, a strain-based failure criterion, rather than stress-based, is sought in terms of the maximum plastic strain in the sidewall, where the failure is predicted to occur.

Figure 8 shows the variations of the pressure level and the volume ductility, respectively, as functions of the maximum equivalent plastic strain ($\varepsilon_{pl,max}$) when the specimen is pressurized. It is apparent that the pressure varies slowly after the specimen is yielded. On the other hand, the plastic strain continues to rise in a nearly linear manner. In fact, the data point can be fit to an equation with very high least-square ($R^2 > 0.999$):

$$\Delta V/V_o = 1.25\ \varepsilon_{pl,max}$$

Therefore, for a general strain-based burst criterion, the following expression is proposed:

$$C = \frac{\Delta V/V_o}{\varepsilon_{pl,max}} = \text{constant}$$

The proportional constant, C, may be a function of vessel geometry, material of construction, and tritium service history. In the present case, C= 1.25 and $\varepsilon_{pl,max}$ = 22%.

Note that this $\varepsilon_{pl,max}$ is less than the limit of uniform elongation denoted by ε_{UTS} (the strain corresponding to UTS), which is about 32% as shown in the inset of Figure 7. The correlation between $\varepsilon_{pl,max}$ and ε_{UTS} has not been established. However, ε_{UTS} is often used for failure criterion to avoid unstable, local necking, and is used as a crucial material performance indicator. Additional material testing for tritium exposed materials and burst tests for vessels with matching material conditions are recommended to provide verification of the methodology for aged materials systems.

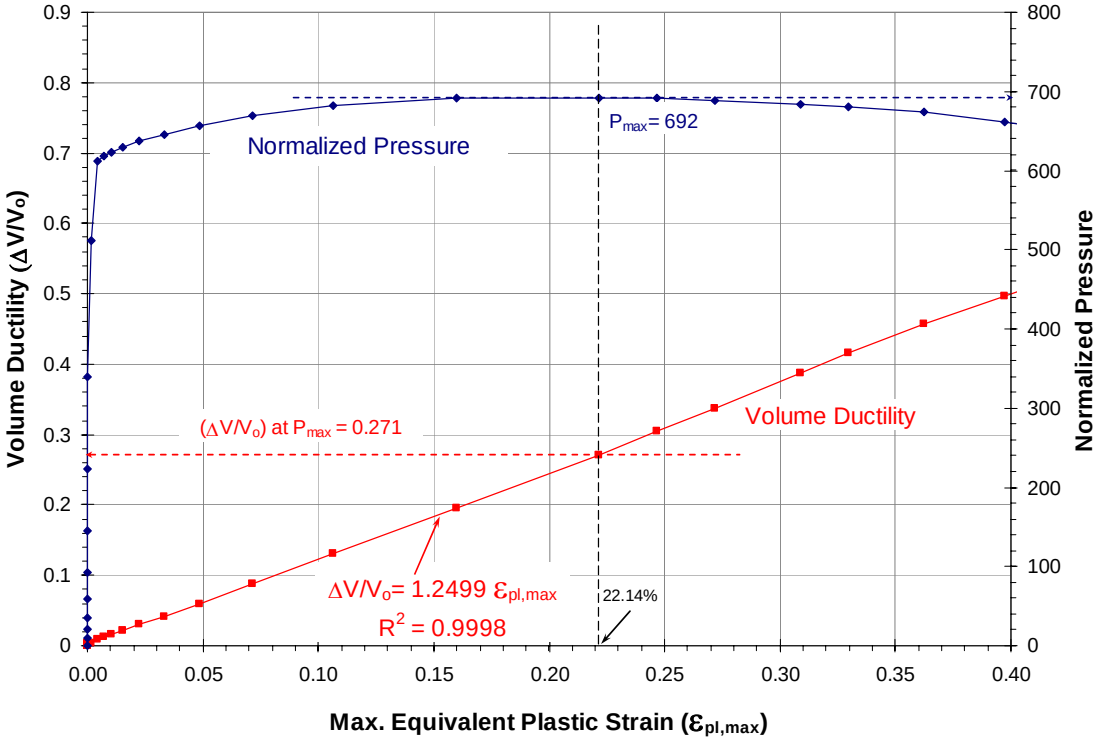

Figure 8 Burst pressure and volume ductility as functions of maximum plastic strain in the test specimen sidewall

PREDICTION OF TRITIUM-EXPOSED VESSELS

It is speculated that the failure of tritium-exposed vessels under burst test occurs soon after the mudflat cracks[3] are formed in the inside wall where tritium absorption,

[3] In a cylindrical vessel under extended tritium service, the mudflat cracks are numerous axial cracks which may be initiated at high pressure in the inside diameter of the circular cross-section and grow radially into

diffusion, and decay to helium-3, occur. It may also be reasonable to assume that these cracks are initiated at the yield stress of the exposed material. In the absence of tested tensile properties for the exposed material in the inside wall of the vessel, the material stress-strain curve is constructed to reflect the helium-3 concentration-dependent tensile properties reported by Robinson [5,6]. In addition, to account for the loss of load carrying capacity of the material after the mudflat cracks are formed under internal pressure, it is assumed that the material behaves elastic-perfectly plastically with a reduced Young's modulus.

A fine-meshed finite element model was used in this part of analysis to provide a better transition of the tensile properties from the exposed (inside wall) to the unexposed states (outside wall). This model contains 3544 elements and 3564 nodes, with 20 elements across the thickness of the sidewall. Both axisymmetric and hydrostatic fluid elements were used, as discussed earlier.

Exposed Material – Helium-3 Concentration-Dependent Tensile Properties

The tritium effects on the tensile properties have been investigated extensively (e.g., [5-8]) but are incomplete due to many variables such as the source of helium and various exposure scenarios. Typically, a stainless steel responds to tritium exposure by increasing the flow stress slightly, but the ductility is reduced markedly, due to the presence of decay helium-3 and hydrogen embrittlement. This phenomenon appears more pronounced in the annealed material than in the high energy rate forged (HERF) steel [7].

Robinson [5,6] reported the effects of tritium and decay helium on tensile properties for austenitic stainless steels HERF 304L, 316, and 21-6-9. The miniature tensile specimens were charged with tritium and allowed sufficient time to saturate the gage section. Various aging times were used for the accumulation of helium-3 resulting from tritium decay. The tensile properties as functions of helium concentration can be found in Reference [5]. The yield stress and UTS are elevated as the helium concentration increases, while the uniform elongation, total elongation, and reduction of area are decreased. Note that the charged tritium was not totally removed from these tensile specimens before testing.

Table 1 summarizes the tensile properties that were extracted from the test results in Reference [5] with helium concentration at 0, 125, 250, and 500 APPM. The zero helium concentration was achieved with the hydrogen-charged specimens [5,6]. A set of simplified true stress-true plastic strain curves can be constructed (Fig. 9). These stress-plastic strain curves are linear because only the yield stress and the (true) UTS data points are available. The failure point for each stress-strain curve can not be identified because the failure stresses were not reported in References [5,6]. Therefore, the range of validity

---

the vessel wall in the thickness direction, but arrested near the degraded (exposed) material boundary. As the internal pressure continues to increase, one of the mudflat cracks, in probabilistic sense, may eventually advance through the vessel wall to form a single, catastrophic crack as seen in the burst test.

of the stress-strain curves in Figure 9 is up to the UTS, and no Bridgman correction is needed.

Table 1 Tensile property of HERF 316 due to helium concentration

Helium Concen-tration	Yield Stress	UTS (Engi-neering)	UTS (True)	Uniform Elonga-tion	Uniform Elongation (ε_{UTS})	Total Elonga-tion	Reduction of Area
(appm)	MPa (ksi)	MPa (ksi)	MPa (ksi)	(engi-neering)	True	(engi-neering)	(engi-neering)
0	530 (77)	670 (97)	878 (127)	0.31	0.27	0.50	0.80
125	550 (80)	680 (99)	877 (127)	0.29	0.25	0.45	0.71
250	570 (83)	690 (100)	876 (127)	0.27	0.24	0.40	0.66
500	630 (91)	725 (105)	891 (129)	0.23	0.20	0.31	0.58

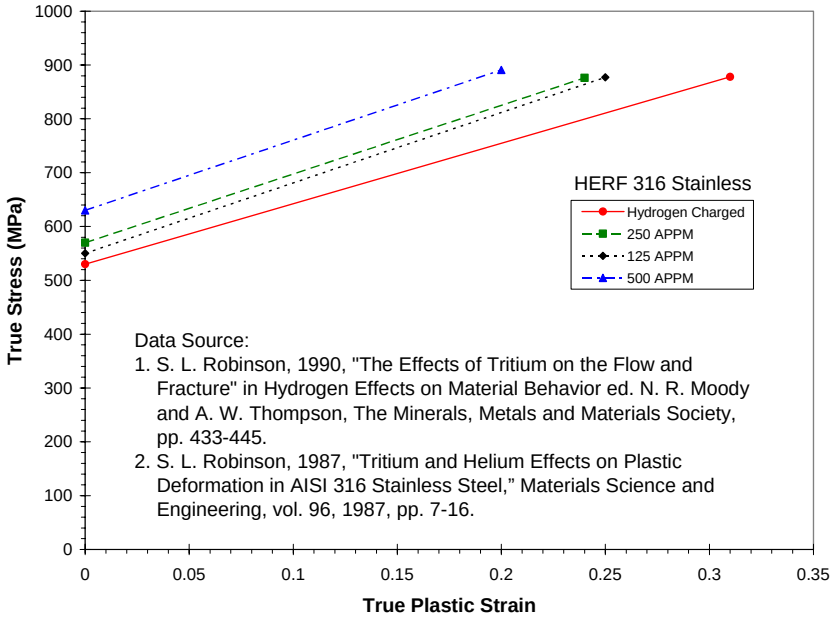

Figure 9 Simplified stress-strain curves for exposed HERF 316 at various helium concentrations

To be consistent with this material data set from Reference [5], the tensile properties for the hydrogen-charged-only (the lowest stress-strain curve in Fig. 9) is applied to the unexposed portion of the vessel in the finite element analysis. As a first order approximation for the mudflat cracks occurring in the exposed material (with helium concentrations of 125, 250, and 500 APPM, respectively, see Fig. 9) under internal

pressure loading, the elastic-perfectly plastic material response was adopted with an arbitrarily reduced Young's modulus (to about ½ of its original value) to account for the loss of load-carrying capacity due to cracking. This treatment was achieved by invoking the ABAQUS User's Subroutine "USDFLD" [1]. A more reasonable approximation was carried out to set a low stiffness in the circumferential direction of the vessel (anisotropic formulation), but was resulted in numerical difficulties during the analysis. Note that the corresponding yield stresses are 550, 570, and 630 MPa (80, 83, and 91 ksi), respectively, for the exposed material containing helium-3 with 125, 250, and 500 APPM (Table 1). The strain hardening portion of the stress-strain curves in Figure 9 for helium-bearing materials was not used when cracking occurs.

A parametric study was performed for the depths of tritium penetration (0, 20, 40, and 60% of the sidewall thickness) at each helium concentration level. The calculated result is shown in Figure 10 for the case of 500 APPM. It represents the evolution of volume change and the internal pressure during the burst test. These figures (Fig. 10 for 500 APPM and similar ones for 125 and 250 APPM) are used to determine the burst pressure and the corresponding volume ductility for each of the case. Note that the volume change and the cavity pressure of the specimen are normalized, respectively, by those for the zero-helium concentration case (hydrogen charged only), for which the burst pressure is 77 MPa (11.16 ksi) and $\Delta V/V_o$ is 0.286. It can be seen that the predicted burst pressures are within 5% of that for the helium-free material. However, the presence of helium significantly reduces the volume ductility. The relationship between the volume ductility and the helium concentration for various depths of tritium penetration can be seen in Figure 11, which can be used to determine the volume ductility for an exposed vessel without knowing its service history as long as helium-3 concentration can be estimated.

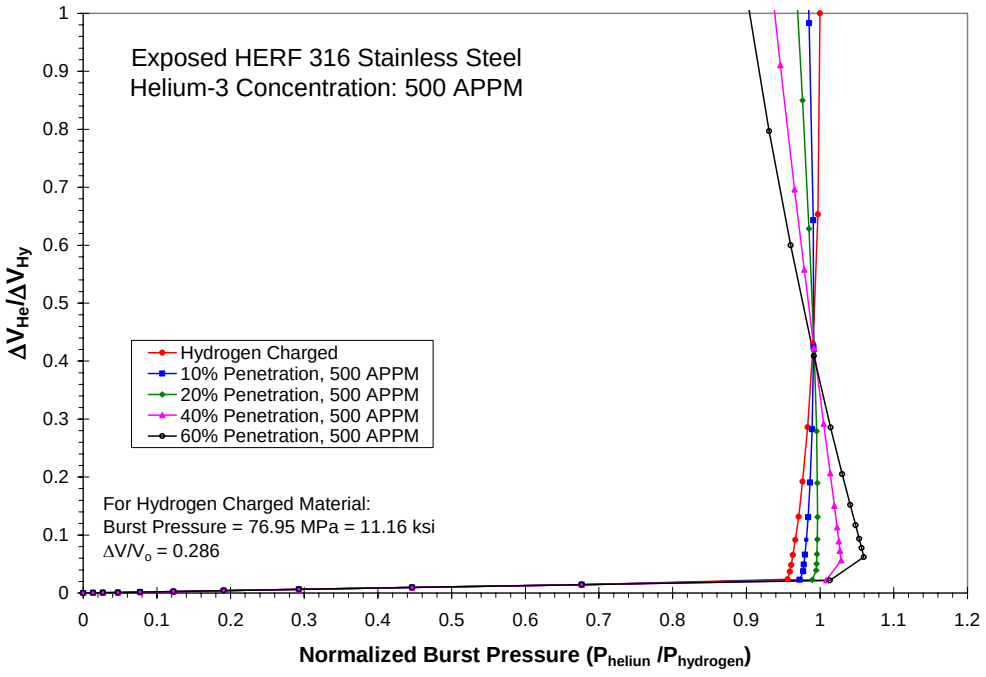

Figure 10 Determination of volume reduction and burst pressure for helium concentration 500 APPM at various depths of penetration

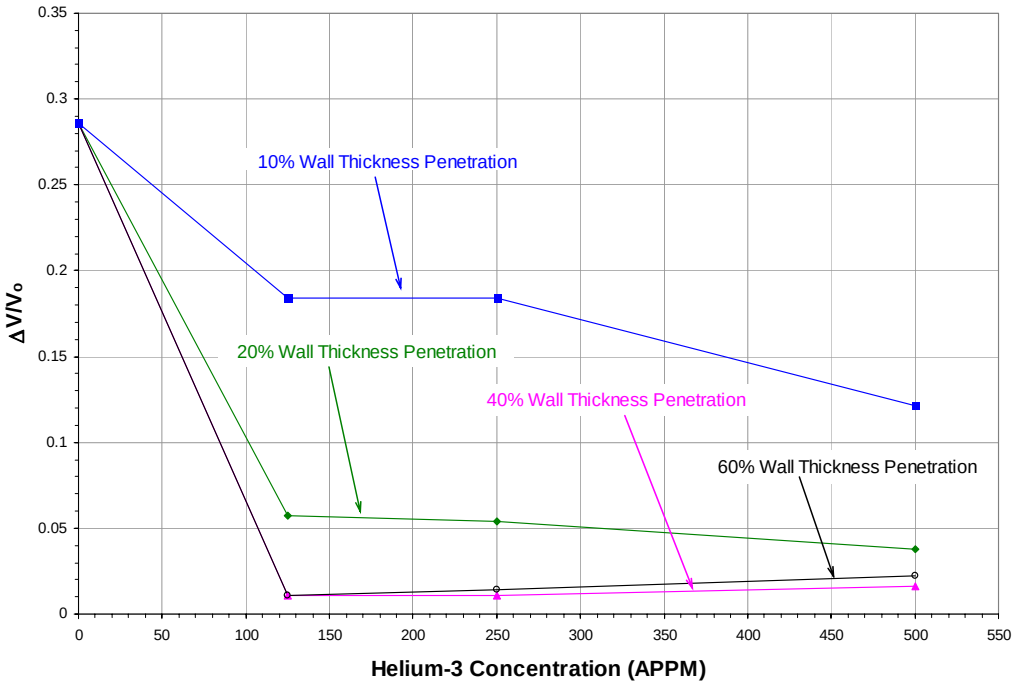

Figure 11 Volume reduction as a function of helium concentration for various depths of penetration

It would be interesting to note that the material in the inner sidewall, where the tritium and helium are both present, may sometimes carry higher load (stress) as seen in Figure 12a for the case of high helium concentration (500 APPM) and deep tritium penetration (60%). This is caused by the elevated flow stress (Table 1). However, this material is penalized by the lower ductility (Table 1) while the plastic strain remains high in the inner sidewall (Fig. 12b). From the current formulation of the material constitutive law (Fig. 9), it seems that there is a subtle balance among the flow stress, ductility, and the depth of penetration. This may explain the unexpected behavior of $\Delta V/V_o$ at higher helium concentration with deep thickness penetration (> 40%, see Fig. 11). On the other hand, for an actual tritium vessel in service, deep tritium penetration with high helium concentration in the sidewall may be unlikely to occur. Figure 12 is used for illustration purpose.

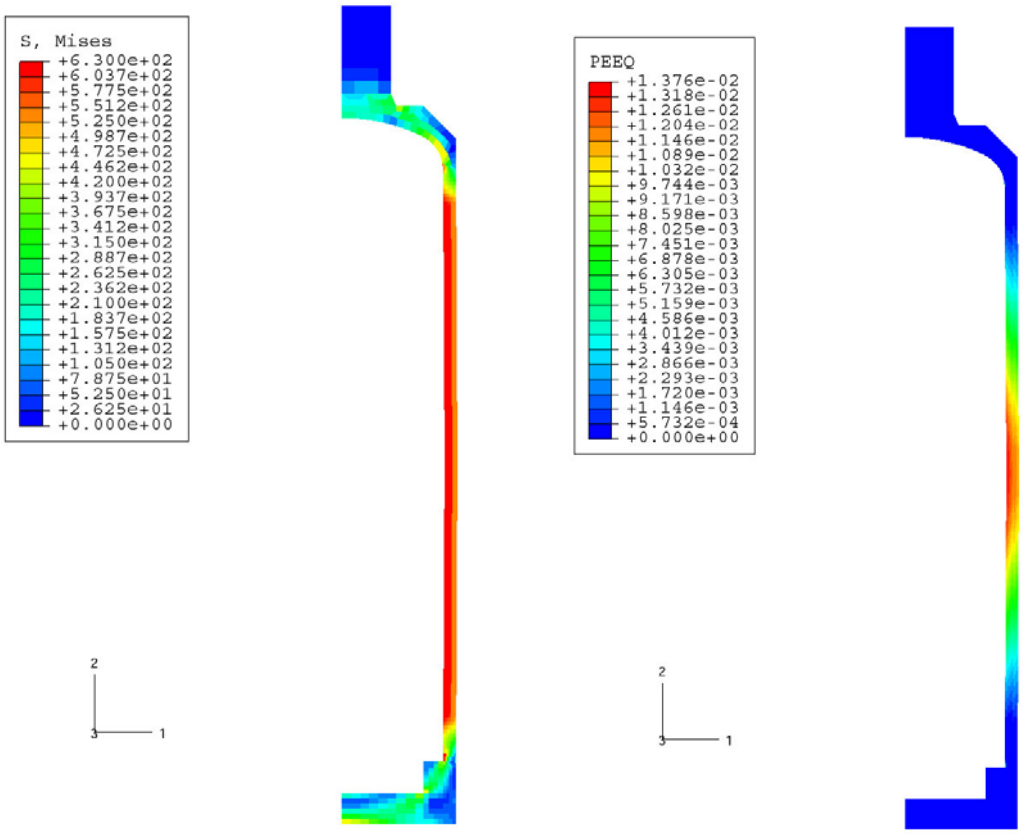

(a) (b)

Figure 12 Contours of (a) Mises stress in MPa and (b) equivalent plastic strain (PEEQ) in a test specimen with 60% of sidewall thickness containing helium with helium concentration of 500 APPM

DISCUSSION AND CONCLUSIONS

The finite element procedure developed in the present work has demonstrated that the burst pressure and volume ductility can be predicted for unexposed tritium vessels (Fig. 7). However, for the vessels that have been in tritium service, only qualitatively consistent results can be reported, that is, the burst pressures remain similar but the ductility is significantly reduced as the exposure time increases. A strong dependence of volume ductility on the helium concentration has been shown. For example, when a uniform distribution of helium with 100 APPM penetrating 20% of the vessel inside wall, the volume ductility is only 1/3 of that for a helium-free material (Fig. 11).

Because the tritium and helium concentration profiles are functions of the initial condition, duration of aging, and the off-gas temperature, etc., the detailed fabrication information and service history are essential to create a realistic finite element model with an appropriate material idealization for accurate prediction of the burst properties. A systematic approach with a carefully selected test matrix, and a complete material property database should be developed.

All burst tests for the exposed vessels show the presence of multiple crack networks on the inside wall. These part-through wall cracks are oriented longitudinally in the case of cylindrical vessels. The lack of understanding of the cracking process poses a serious difficulty in accurate prediction of tritium-affected burst properties. The experimental observations and the present analysis strongly suggest that the crack nucleation and the depth of propagation play important roles in the marked decrease of burst volume ductility for the exposed vessels. In order to further improve the modeling prediction capability, experimental efforts are needed to determine the cracking mechanism under burst test conditions. This may be achieved by a series of testing of identically exposed vessels, each subjected to different pressure level up to burst, and followed by destructive examination for cracking. Alternatively, by interrupting a single burst test which is coupled with acoustic emission and nondestructive ultrasonic examinations, the crack initiation can be monitored and the subsequence crack growth can be sized. The numerical procedure to simulate the mechanical response of the cracked material can then be formulated after the cracking event is properly characterized.

ACKNOWLEDGMENTS

The authors wish to acknowledge the support from the U. S. Department of Energy (DOE) Savannah River Site (SRS) Plant-Directed Research and Development (PDRD) program to the Savannah River National Laboratory (SRNL), funded by DOE under Contract No. DE-AC09-96SR18500.

REFERENCES

[1] ABAQUS General Purpose Finite Element Program, ABAQUS Inc., Providence, Rhode Island.
[2] Bridgman, P. W., 1944, “The Stress Distribution at the Neck of a Tension Specimen,” Transactions of American Society for Metals, vol. 32, pp. 553-574.
[3] Dowling, N. E., 1993, Mechanical Behavior of Materials: Engineering Methods for Deformation, Fracture, and Fatigue, Prentice Hall, Englewood Cliffs, New Jersey.
[4] Zhang, Z. L., Hauge, M., Ødegård, and Thaulow, C., 1999, “Determining material true stress-strain curve from tensile specimens with rectangular cross-section,” International Journal of Solids and Structures, Vol. 36, pp. 3497-3516.
[5] Robinson, S. L., 1990, "The Effects of Tritium on the Flow and Fracture of Austenitic Stainless Steels", in Hydrogen Effects on Material Behavior, ed. A. W. Thompson and N. R. Moody, The Minerals, Metals & Materials Society, pp. 433-445.
[6] Robinson, S. L., 1987, "Tritium and Helium Effects on Plastic Deformation in AISI 316 Stainless Steel,” Materials Science and Engineering, vol. 96, pp. 7-16.
[7] Morgan, M. J., 1990, “The Effects of Hydrogen Isotopes and Helium on the Flow and Fracture Properties of 21-6-9 Stainless Steel,” Proc. Fine Symposium, ed. P. K. Liaw, J.R. Weertman, H. L. Marcus, and J. S. Santner, Warrendale, PA., TMS, pp. 105-111.
[8] Louthan, Jr., M. R., 2001, “Tritium Decay, Irradiation and Hydrogen/Helium Effects on Type 316L Austenitic Stainless Steel,” WSRC-MS-2001-00040, Westinghouse Savannah River Company, Aiken, South Carolina.